



Available online at [www.sciencedirect.com](http://www.sciencedirect.com)



Reliability Engineering and System Safety 00 (2014) 1–20

Reliability  
Engineer-  
ing &  
System  
Safety

## Coupling mode-destination accessibility with a quantitative seismic-risk assessment to identify at-risk communities

Mahalia Miller<sup>a</sup>, Jack W. Baker<sup>a</sup>

<sup>a</sup>*Stanford University, Stanford, CA USA*

---

### Abstract

In this paper, we develop a framework for coupling mode-destination accessibility with a quantitative seismic-risk assessment to identify communities at a high risk for travel disruptions after an earthquake. For a case study of the San Francisco Bay Area, we find that accessibility varies more strongly from location to location than between income classes, and we identify particularly at-risk communities. We also observe that communities more conducive to local trips by foot or bike are predicted to be less impacted by losses in accessibility.

© 2014 Published by Elsevier Ltd.

**Keywords:** Infrastructure, Risk, Earthquakes

---

### 1. Introduction

Seismic risk assessment in earthquake engineering tends to focus on buildings, bridges, and the performance of infrastructure systems. For measuring the performance of transportation systems, researchers typically use engineering-based metrics such as the post-earthquake connectivity loss, which quantifies the decrease in the number of origins or generators connected to a destination node [e.g., 1], or the post-earthquake travel distance between two locations of interest [e.g., 2]. These frameworks have provided insight into seismic vulnerability and possible risk mitigation. However, the link to the human ramifications can be limited.

In the field of vulnerability sciences, researchers have long stressed the importance of the impact on human welfare from earthquakes. For example, Bolin and Stanford write that, “‘Natural’ disasters have more to do with the social, political, and economic aspects than they do with the environmental hazards that trigger them. Disasters occur at the interface of vulnerable people and hazardous environments” [3]. A recent World Bank and United Nations report echoed this idea that the effects on human welfare turn natural hazards into disasters [4].

Historical events emphasize the complex social effects of earthquakes. For example, on one hand the 1994 Northridge earthquake caused major damage to nine bridges, which, while significant, represented only 0.5% of the bridges estimated by Caltrans to have experienced significant shaking [5]. On the other hand, over half of businesses reported closing after the earthquake with 56% citing the “inability of employees to get to work” as a reason [6]. Furthermore, the total economic cost of transport-related interruptions (“commuting, inhibited customer access, and shipping and supply disruptions”) from this earthquake is estimated at 2.16 billion USD (2014) [7], using the consumer price index to account for inflation.

An emergent trend in earthquake engineering related to the social impacts is measuring the cumulative extra time needed for travel after an earthquake, sometimes called travel time delay [e.g., 8, 9]. This performance measure captures basic re-routing due to road closures and enables identifying roads more likely to be very congested. Travel time

23 approximately measures one aspect of impact on people, but does not capture the fact that some destinations and trips  
24 have higher value than others. Furthermore, this approach measures the impacts by focusing on aggregate regional  
25 effects rather than individual communities and demographic groups. Some recent work has looked at other metrics,  
26 such as the qualitative criteria-based metric “disruption index” [10]. However, this does not provide a quantitative link  
27 between the technical impact and the human ramifications. Other work has looked at resiliency, but defined it in pure  
28 engineering terms, such as percentage of a simplified road network that is functional [11]. Outside of transportation  
29 systems, some researchers have investigated the interplay between earthquake damage, such as damage to the electric  
30 power and wastewater networks, and the usability of houses and other buildings; this represents an important first  
31 step [12].

32 In contrast to the work on transportation-related seismic risk, urban planning has a long tradition of studying the  
33 impact on people of events and policy [13]. Accessibility is one metric popular in urban planning to measure  
34 the impact of different transportation network scenarios, and it measures how easily people can get to desirable  
35 destinations, which is one measure of social impact [14]. Furthermore, accessibility, by definition, quantifies one  
36 key aspect of human welfare [e.g., 14]. Within urban planning, accessibility has been measured in many ways,  
37 including individual accessibility, economic benefits of accessibility, and mode-destination accessibility [15]. The  
38 mode-destination accessibility is computed by taking the log value of the sum of a function of the utilities of each  
39 destination over all possible destinations and travel modes, where the utility decreases if getting to that destination is  
40 more costly or time-intensive [16]. This choice of accessibility definition is particularly applicable to quantifying the  
41 impacts of catastrophes, such as earthquakes, because certain destinations might be more critical for people in certain  
42 locations or from different socio-economic groups (such as low income or high income). However, this accessibility  
43 measure has not yet been linked to risk assessment. In addition, the majority of work to date assumes that travel  
44 demand and mode choice will remain unchanged after a future earthquake, which historical data suggests is not the  
45 case [7]. A first step towards considering variable demand is work in the literature that varies demand by applying a  
46 constant multiplicative factor on all pre-earthquake travel demand [8].

47 In this paper, we develop a framework for coupling mode-destination accessibility with a quantitative seismic-risk  
48 assessment to identify at-risk populations and measure the accompanying impacts on human welfare. We illustrate our  
49 approach with a case study of the San Francisco Bay Area transportation network, including highways, local roads,  
50 and public transportation lines. This study analyzes a set of forty hazard-consistent earthquake scenarios, ground-  
51 motion intensity maps, and damage maps, as we introduced in [20] using the optimization procedure we proposed  
52 in [18]. For each of these damage maps, we model damage with a practical, agent-based transportation model used by  
53 the local transportation authorities that includes damage to bridges, roads, and transit lines, and varies demand. Then,  
54 with this model, we estimate the predicted losses in accessibility according to 12 socio-economic groups used by local  
55 planners for the case study region, based on income class, and ratio of personal vehicles to workers in a household.

56 **2. Case study: San Francisco Bay Area**

57 **2.1. Case study overview**

58 We focus on the San Francisco Bay Area, a seismically-active region, to illustrate our approach (Figure 1). The  
 59 area follows a polycentric metropolitan form, with San Francisco as the primary center and other jobs concentrated  
 60 in suburban centers, such as Silicon Valley [19]. The region has a wide array of trip patterns for mandatory and  
 61 non-mandatory trips. Furthermore, trip times and routes vary greatly depending on travel preferences and workplace  
 62 locations [19]. Thus, we might expect noticeable disparities between households in the risk of travel time delays due  
 63 to earthquakes.

64 This analysis considers the complex web of roads and transit networks of the case study area. The roads are  
 65 modeled by a directed graph  $G = (V, E)$ , where  $V$  is a finite set of vertices representing intersections, and the set  $E$ ,  
 66 whose elements are edges representing road links, is a binary relation on  $V$ . In this model,  $(|V|, |E|) = (11,921, 32,858)$   
 67 including centroidal links and  $(|V|, |E|) = (9,635, 24,404)$  without. Centroidal links do not correspond to particular  
 68 physical roads but instead capture more subtle travel flows, such as from outside the study area or the flow of people  
 69 to and from some minor local roads. We also model 43 transit networks, as detailed in [20].

70 We model damage from ground shaking intensity to a set of 1743 highway bridges impacting the road and some  
 71 transit networks, with data provided by the California Department of Transportation (Caltrans), and 1409 structures  
 72 impacting the rapid transit network, BART, with data provided by that agency. We refer readers to [20] for more  
 73 details about matching these structures, hereafter called components, to the relevant road and transit networks.

74 **2.2. Ground-motion intensity maps**

75 **2.2.1. Theory**

76 We now describe how to produce a set of maps with ground-motion intensity realizations at each location of  
 77 interest in a region and corresponding occurrence rates that reasonably capture the joint distribution of the ground-  
 78 motion intensity. First, we generate  $Q$  earthquake scenarios from a seismic source model. The seismic source model  
 79 specifies the rates at which earthquakes of specified magnitudes, locations, and faulting types will occur. This set of  
 80 earthquake scenarios is comparable to a stochastic event catalogue in the insurance industry.

81 Second, for each earthquake scenario in the seismic source model, we use an empirical ground-motion prediction  
 82 equation (GMPE) [e.g., 21, 22, 23, 24] to model  $Y$ , the resulting intensity measure at each location of interest [e.g.,  
 83 25, 26].

84 Then, for each of the  $Q$  earthquake scenarios, we sample  $b$  realizations of the spatially-correlated ground-motion  
 85 intensity residual terms. Readers are referred to [27] for a survey of sampling methods. Once residuals are sampled,  
 86 the total log ground-motion intensity ( $Y$ ) is computed as

$$\ln Y_{ij} = \overline{\ln Y(M_j, R_{ij}, V_{s30,i}, \dots)} + \sigma_{ij}\epsilon_{ij} + \tau_j\eta_j \quad (1)$$

87 where  $j$  is the ground-motion intensity map index ( $j = 1, \dots, m$  where  $m = Q \times b$ ),  $\epsilon_{ij}$  is the normalized within-event  
 88 residual in  $\ln Y$  representing location-to-location variability and  $\eta_j$  is the normalized between-event residual in  $\ln Y$   
 89 and the other parameters are defined above. Both  $\epsilon_{ij}$  and  $\eta_j$  are normal random variables with zero mean and unit  
 90 standard deviation. The vector of  $\epsilon_{ij}$  can be modeled by a spatially-correlated multivariate normal distribution [e.g.,  
 91 28] and the  $\eta_j$  by a standard univariate normal distribution.

92 The result is a set of  $m$  ground-motion intensity maps (e.g., Figure 2(a)). Since we simulate an equal number  
 93 ( $b$ ) of ground-motion intensity maps per earthquake scenario, the annual rate of occurrence for the  $j^{\text{th}}$  ground-motion  
 94 intensity map is the original rate of occurrence of the earthquake scenario, divided by  $b$ . We denote the final result as  
 95  $w_j$ .

96 **2.2.2. Implementation**

97 To generate a stochastic catalog of ground-motion intensity maps, we use the OpenSHA Event Set Calculator [29].  
 98 This software outputs the mean,  $\overline{\ln Y_{ij}}$ , and standard deviation values,  $\sigma_{ij}$  and  $\tau_j$ , for all locations of interest for a  
 99 specified seismic source model and ground-motion prediction equation. The intensity measure is the 5%-damped  
 100 pseudo absolute spectral acceleration ( $Sa$ ) at a period  $T = 1\text{s}$ , which is the required input to the fragility functions  
 101 below. This spectral acceleration value represents the maximum acceleration over time that a linear oscillator with



Figure 1. Study area: San Francisco Bay Area, CA with specific travel analysis zones (TAZs) used in the case study marked in blue.

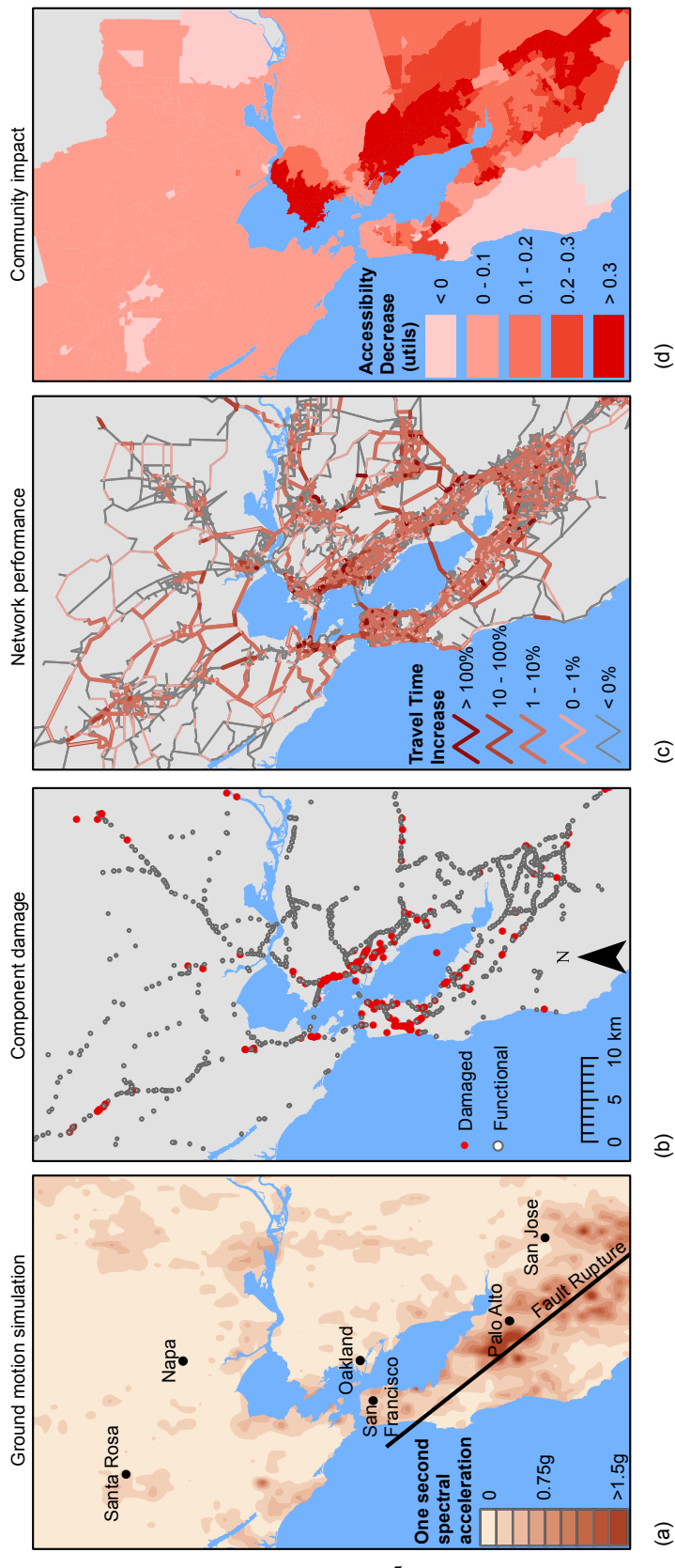


Figure 2. Illustration of the risk framework for one earthquake event including a) One-second spectral acceleration (ground-motion intensity) map with earthquake rupture, b) bridge (component) damage map, c) map of travel time increase (network-performance measure) values, and d) map of accessibility values averaged over all market segments by travel analysis zone (TAZ). There are 1454 TAZs.

102 5% damping and a period of 1 second will experience from a given ground motion. We calculate these values at  
 103 each component location (bridges and other structures). Using one ground-motion intensity measure per component  
 104 is a common simplification of the time-varying acceleration dynamics [e.g., 30, 9] that may have lower errors for  
 105 components with a natural period near 1 second as opposed to long-span bridges. We use the UCERF2 seismic source  
 106 model [31], Wald and Allen topographic slope model for the shear wave velocity  $V_{s30,i}$  [32], and the Boore and  
 107 Atkinson [21] ground-motion prediction equation. Using this seismic source model, which is then discretized into  
 108 a list of faults and a stratified list of magnitudes and rupture locations for each, we obtain a set of 2110 earthquake  
 109 events on all active faults, each with an annual occurrence rate greater than or equal to  $10^{-5}$ . We simulate the sets  
 110 of maps by combining the mean terms from the Event Set Calculator and spatially-correlated residual terms of the  
 111 ground-motion intensity (using [28]) according to the basic ground-motion model, Equation 1.

### 112 2.3. Damage maps

#### 113 2.3.1. Theory

114 Calculating network performance risk requires assessing the structural damage of relevant components after future  
 115 earthquakes. The link between ground-motion intensity and structural damage is often provided by fragility functions.  
 116 Fragility functions express  $P(DS_i \geq ds_S | Y_{ij} = y)$ . We assume one component, such as a bridge, per site location, so we  
 117 will identify both components and site locations via the index  $i$ . Using that notation,  $DS_i$  is a discrete random variable  
 118 whose value represents the damage state for the  $i^{th}$  component and  $ds$  is a damage state threshold of interest. The  
 119 damage state is conditioned on a realization,  $y$ , of the random variable  $Y_{ij}$ , the ground-motion intensity at the  $i^{th}$  site  
 120 and  $j^{th}$  ground-motion intensity map. Researchers have calibrated fragility functions using historical post-earthquake  
 121 data [e.g., 33], experimental and analytical results [e.g., 34], hybrid approaches, and expert opinion. It is possible to  
 122 sample the damage states from a joint distribution that includes correlation, such as due to similarities in design or  
 123 construction practices [e.g., 35].

124 By sampling a damage state for each component, with probabilities obtained from the fragility functions given  
 125 the ground-motion intensity, we produce a damage map (e.g., Figure 2(b)). The damage map has a realization of the  
 126 damage state of each relevant component. This sampling process can be repeated multiple times to simulate multiple  
 127 damage maps per ground-motion intensity map. For example, if equal numbers of damage maps are sampled per  
 128 ground-motion intensity map ( $c$  damage maps per ground-motion intensity map), the weight of the  $j^{th}$  damage map  
 129 should be adjusted accordingly to  $w_j$ , where  $w_j = \frac{w_j}{c}$ , and  $j' = 1, \dots, J$ .

130 *Functional percentage* relationships link the component damage to the functionality of network elements. For  
 131 example, in a road network, when a bridge collapses, the traffic flow capacity of the road it carries and it crosses can  
 132 be modeled as reduced to zero. These relationships are often derived from a combination of observation and expert  
 133 opinion, often due to data scarcity [36]. Furthermore, the relationships are typically deterministic for a certain com-  
 134 ponent damage state and restoration time [36]. Thus, in this paper, each damage map corresponds to a functionality  
 135 state for every element of the network.

#### 136 2.3.2. Implementation

137 *Component damage.* We use fragility functions of the following form to provide the link between ground-motion  
 138 shaking and component damage:

$$P(DS_i \geq ds_S | Y_{ij} = y) = \Phi\left(\frac{\ln y - \lambda_{\xi,i}}{\xi_{\xi,i}}\right), \quad (2)$$

139 where  $\Phi$  is the standard normal cumulative distribution function,  $\lambda_{\xi,i}$  and  $\xi_{\xi,i}$  are respectively the mean and standard  
 140 deviation of the  $\ln Y_{ij}$  value necessary to cause the  $\xi^{th}$  damage state to occur or be exceeded for the  $i^{th}$  component,  
 141 and the other variables are defined above. By using the previous equation and the inverse method, we can sample  
 142 realizations of component damage states for a given ground-motion intensity.

143 The California Department of Transportation (Caltrans) provided the fragility function values  $\lambda_{\xi,i}$  and  $\xi_{\xi,i}$  used  
 144 in this study for the highway components in summer 2012, which was last updated in 2007 and includes various  
 145 retrofitted bridges [37]. The  $\lambda_{\xi,i}$  values are based on component characteristics including number of spans and age  
 146 as detailed in [33]. The  $\xi_{\xi,i}$  values are given as a constant. The BART seismic safety group provided the fragility  
 147 function values  $\lambda_{\xi,i}$  and  $\xi_{\xi,i}$  used in this study for the BART-related components for the state of the network in summer  
 148 2012. At that time, data was available for the aerial structures shown in Figure ???. These correspond to the safety

149 performance goals under the recent retrofit program [38]. The numbers are comparable to the Caltrans fragility data.  
 150 For the BART components, however,  $\xi_{\zeta,i}$ , the standard deviation of the  $\ln S_a$  value necessary to cause the extensive  
 151 damage state to occur or be exceeded, varies depending on the component. Both sets of fragility functions are based  
 152 on the assumption that damage can be reasonably accurately estimated by the ground motion intensity at each site  
 153 independently, and that the damage state can be reasonably estimated by an analytical model considering a single  
 154 ground-motion intensity measure. In addition, the fragility curves do not directly consider the effects of degradation.  
 155 Current work is ongoing to refine these assumptions [e.g., 34, 39, 40].

156 Caltrans also provided other component properties such as length, construction year, construction materials, out-  
 157 to-out distance (the maximum distance in the perpendicular direction to traffic flow), number of spans, and average  
 158 daily traffic flow). Similarly, Caltrans provided estimates for bridge replacement costs in current (2014) USD: 175 per  
 159 square foot for construction and 10 per square foot for demolition of the damaged bridge [41].

160 Per ground-motion intensity map, we sample 1 damage maps (e.g., Figure 2(b)), which each has a realization of  
 161 the component damage state at each component location according to the fragility function (eq. 2). The provided  
 162 fragility functions do not consider correlation of the structural capacities, but other models could be used [e.g., 35].

163 *Transit network damage.* Each of the 43 transit systems we considered will be impacted differently. For Caltrain,  
 164 conversations with managers suggest that given that there is one shared track system, the system would either be  
 165 fully operational or not at all. Similarly, managers suggested modeling the VTA system as fully functional or not.  
 166 Depending on where the BART train cars are when the earthquake strikes, the agency could accommodate different  
 167 emergency plans. However, BART representatives suggested considering that if any part of a route is damaged, the  
 168 entire corresponding route would not be operational (but other routes on different tracks might be still operational). In  
 169 other words, each BART route as well as the Caltrain and VTA routes are each a weakest-link system, so the failure  
 170 of a single component will cause the route to be non-operational. We modeled the ferry systems as fully functioning  
 171 for all earthquake events. For all earthquake events including the baseline, trans-bay and cross-county bus lines were  
 172 discontinued, but main lines in urban areas as well as other local bus networks were maintained per recommendations  
 173 from the MTC, though they may face delays due to traffic congestion.

174 *Road network damage.* Each component damage state maps directly to the traffic capacity on associated road seg-  
 175 ments. We use a functional percentage relationship to compute the traffic capacity of relevant road segments. Based  
 176 on discussions with Caltrans, we consider travel conditions one week after an earthquake, since it is a critical period  
 177 for decision making. For example, one week after most events, bridges should have been inspected and surface dam-  
 178 age should be repaired, but major reconstruction would not have yet begun. According to our functional percentage  
 179 relationship, at this point in time, the components have one of two classes of functionality, zero traffic capacity and  
 180 full traffic capacity [36]. We can thus summarize the component damage using two damage states  $ds_s$ ,  $ds_{damaged}$  and  
 181  $ds_{functional}$ , which correspond to the common HAZUS *extensive* or *complete* damage states and the *none*, *slight*, or  
 182 *moderate* damage states respectively [36]. Thus, the functional percentage relationship assigns zero traffic capacity  
 183 on road segments that have at least one component in the  $ds_{damaged}$  damage state, and full traffic capacity otherwise.  
 184 We do not consider network damage from sources other than main structural damage from ground shaking, such as  
 185 tunnel displacement or liquefaction, but the framework allows including such considerations. In the discussion below,  
 186 we consider a set of 113,940 damage maps, which correspond to 2110 scenarios, 3 ground-motion intensity maps per  
 187 scenario, and 18 damage maps per ground-motion intensity map.

## 188 2.4. Network performance

### 189 2.4.1. Theory

190 The final step for the event-based risk analysis is to evaluate the network performance measure,  $X$ . For this  
 191 application, we consider a metric popular in urban planning, *mode-destination accessibility change* [e.g., 15, 42, 43]  
 192 (e.g., Figure 2(d)). Mode-destination accessibility, hereafter referred to as accessibility, measures the distribution of  
 193 travel destination opportunities weighted by the composite utility of all modes of travel to those destinations, i.e.,  
 194 the ease of someone getting to different destinations weighted by how desirable those destinations are [16, 14]. The  
 195 utility function for the mode-destination choice may be estimated using a multinomial random utility model where

196 the logsum represents the accessibility value [44, 16, 14]. Namely, accessibility for a particular agent  $a$  is

$$Acc_a = \ln \left[ \sum_{c \in C_a} \exp(V_{a(c)}) \right], \quad (3)$$

197 where  $V_{a(c)}$  is the utility of the  $c^{th}$  choice for the  $a^{th}$  person for  $a = 1, \dots, A$ , and  $C_a$  is the choice set for the  $a^{th}$   
 198 person [16]. Choices refer to travel destinations and the mode of travel (driving, walking, bus, etc.). The units are a  
 199 dimensionless quantity, *utils*. As an extension, the accessibility values from the previous equation can be converted  
 200 into equivalent time and dollar amounts using *compensating variation* for cost-benefit studies; for the case study,  
 201 0.0134 *utils* (generic measure of utility) equals the value of one minute per day [14, 45, 46] and we conservatively  
 202 value one hour of time as approximately \$15 [47]. In other words, one *util* is worth approximately \$20 per person per  
 203 day based on these assumptions. With nearly 7 million people in the region, even small changes in *utils* lead to large  
 204 economic losses. Since accessibility measures how easily people can get to the destinations they desire, accessibility  
 205 is used as one of the measures of human welfare [e.g., 14].

206 Once the chosen performance measure is computed for each damage map, we aim to estimate the exceedance  
 207 rate of different levels of performance. The annual rate,  $\lambda$ , of exceeding some threshold of network performance  
 208 is estimated by summing the occurrence rates of all damage maps in which the performance measure exceeds the  
 209 threshold:

$$\lambda_{X \geq x} = \sum_{j=1}^J w_j \mathbb{I}(X_j \geq x) \quad (4)$$

210 where  $x$  is an accessibility value threshold of interest and  $X_j$  is the accessibility value realization for the  $j^{th}$  damage  
 211 map. The variable  $w_j$  is the occurrence rate of the  $j^{th}$  damage map. The indicator function  $\mathbb{I}$  evaluates to 1 if the  
 212 argument,  $X_j \geq x$ , is true, and 0 otherwise. By evaluating  $\lambda$  at different threshold values, we derive an exceedance  
 213 curve (e.g., Figure 6).

#### 214 2.4.2. Implementation

215 We compute accessibility using *Travel Model One* (version 0.3), an activity-based model used for the official San  
 216 Francisco Bay Area travel model by the Metropolitan Transportation Commission (MTC), the local metropolitan plan-  
 217 ning organization (MPO) [48]. It represents the full road network as well as the public transit networks, biking, and  
 218 walking. Travel demand data consists of the locations of different households in the case study area, their destination  
 219 preferences and utilities, their number of vehicles, their income and other demographic data [48, 46]. More details can  
 220 be found in [49]. This data was collected by the MTC from surveys and census information. Thus, we assume that the  
 221 distributions of travel preferences do not change after an earthquake, although the actual destinations and trips may  
 222 vary. For example, if a trip takes a very long time after a simulated earthquake, it is less likely that the trip will occur.  
 223 The result is a *variable* travel demand model. This model uses a combination of Java code called CT-RAMP [50],  
 224 and the Citilabs Cube Voyager and Cube Cluster software programs, which are part of a leading commercial software  
 225 suite for transportation planning [48]. This model differs from previous representations of this network [e.g., 9, 51],  
 226 since it includes not only major roads but also local roads and transit lines. We have provided further details about  
 227 computing mode-destination accessibility using this high-fidelity model in [20].

228 This analysis considers 40 interesting and hazard-consistent events, as defined by 40 sets of ground-motion inten-  
 229 sity maps, damage maps, and accessibility performance measure realizations. We selected this set of events with the  
 230 optimization-based procedure we introduced in [18]. Readers are referred to [20] for more details about this set of  
 231 events.

232 In the following sections, we first compare region-wide results, and then focus on particular characteristics of  
 233 three communities (Figure 1 shows the study area and three communities). Finally, we discuss generalizable trends.

Income class	Income range, 1989 USD	Income range, 2014 USD
Low	0 - \$25,000	0 - \$47,334
Medium	\$25,000 - \$45,000	\$47,334 - \$85,202
High	\$45,000 - \$75,000	\$85,202 - \$142,004
Very high	more than \$75,000	more than \$142,004

Table 1. Income class definitions for the case study region, as defined by the local planning organization, the MTC [46] and also translated to current 2014 USD using the consumer price index.

### 234 3. Results and Discussion

#### 235 3.1. Overview of results region-wide

236 In this section, we analyze region-wide trends in accessibility losses for the case study area. As mentioned in  
 237 Section 1, we first analyze each of the 12 socio-economic groups used in practice for the case study region [46], which  
 238 are characterized based on households. The socio-economic groups correspond to all combinations of four different  
 239 income classes (Table 1), and three different classes of automobile availability in the household (zero automobiles,  
 240 fewer automobiles than household members that work, a greater or equal number of automobiles as compared to the  
 241 number of household members that work).

242 We first assess the data availability for each of the segments. Each data point represents a trip by a person of a  
 243 household, who is modeled as an agent in the high-fidelity transportation model. The results suggest comparing house-  
 244 holds with at least one car, because for households without cars (no cars), only the low income class has reasonably  
 245 many trips.

246 General patterns emerge in the expected losses in accessibility. The expected losses are computed by taking  
 247 an average of the accessibility results for each of the 1454 travel analysis zones (TAZ) for each earthquake event,  
 248 weighted by the adjusted annual likelihood of occurrence from the optimization results.

249 First, we notice that the ratio of cars to the number of people who work in a household is correlated with accessi-  
 250 bility risk; a higher ratio corresponds to higher expected decreases in accessibility. This corresponds to going across a  
 251 column in Figure 3. For example, for the first row representing low income households, we notice a marked change in  
 252 accessibility across the columns, as indicated by an expanded area of darkened TAZs from left to right (Figure 3(a-c)).  
 253 Note that 1 *util* corresponds to a consumer value of compensating variation of approximately \$20 per person per day,  
 254 which assumes low (conservative) estimates of the value of time for travel delays and value of getting to destinations.

255 We might expect these households with more cars to take longer trips because there might be a relationship  
 256 between needing to travel longer distances and needing an extra car or two in a household. This is indeed the case,  
 257 but it is not fully predictive. In fact, there is only a weak trend between average trip length for a TAZ before any  
 258 earthquake and the predicted impact on accessibility (Figure 4). Instead, we hypothesize that there are other latent  
 259 variables correlated with car ownership. For example, the geographic distribution of people without cars varies.  
 260 Additionally, in Section 3.5, we will further explore the correlation between the percentage of car-based trips and  
 261 accessibility risk. We will show that TAZs with fewer car-based trips, tend to have lower risk of accessibility losses.

262 Second, controlling for car ownership, we see a fairly equitable distribution of risk across income class segments.  
 263 For example, by looking at households with fewer workers than cars (middle column of Figure 3), the variation from  
 264 TAZ to TAZ is significantly more striking than the difference across income segments (Figure 3(b,e,h,k)). Similarly,  
 265 while trip lengths are slightly longer for higher income households, the differences are subtle.

266 Thus, for a given TAZ, the differences across incomes are not that great. At the same time though, there is  
 267 an unequal geographic distribution of wealth in the San Francisco Bay Area. Because of this, when we aggregate  
 268 accessibility risk across TAZs, we see that accessibility risk rises with increasing household income (Figure 6(b)).  
 269 Therefore, even though the poor are generally the most vulnerable to natural disasters including hurricanes, floods  
 270 and earthquakes, wealthier households in the San Francisco Bay area are more vulnerable than the other income  
 271 groups to earthquake-related accessibility risk.

272 Next, we consider which geographic parts of the San Francisco Bay Area are at an elevated risk. The results show  
 273 regions of high risk: in the East Bay due East of San Francisco, in the suburbs of San Jose, along the coastal and  
 274 Bay-side regions South of San Francisco (Millbrae and Pacifica, e.g.), and in parts of San Francisco (South-Central  
 275 neighborhoods including Westland Highlands and Glen Park neighborhoods). One may have expected more high risk

276 areas on the San Francisco Peninsula, because of the San Andreas fault, which can generate large magnitude events.  
 277 In contrast, the East Bay has higher shaking levels at more moderate return periods, due to the higher relative annual  
 278 frequency of events on the Hayward Fault; this is correlated to bridge damage and thus road closures. Furthermore,  
 279 the data suggests that both the more common moderate-magnitude East Bay events and the rare higher-magnitude  
 280 San Andreas events can cause accessibility problems for the East Bay. Figure 5 shows one sample realization of a  
 281 M6.85 Hayward event and one sample realization of a M7.45 San Andreas event—both follow the general trend of  
 282 high predicted accessibility losses in the East Bay. In contrast, while any events could contribute to the risk in San  
 283 Francisco, our model results show the main accessibility losses in San Francisco corresponding to the San Andreas  
 284 events. Figures 5(c,d) provide one such example. Figures 5(e,f) show an example of a lower magnitude event farther  
 285 away from the main population centers, a M6.35 event in the Great Valley Pittsburg-Kirby Hills Fault. This shows  
 286 how the range of more minor faults in the East Bay can contribute to that area's risk. Also, we have shown the results  
 287 for one socio-economic group in Figure 5, but the other socio-economic groups follow the same general patterns,  
 288 albeit with different specific values.

289 Finally, we can examine the rates of loss exceedance (Equation 4). Figure 6 shows a similar shape to the loss  
 290 exceedance curves for other metrics such as portfolio losses and travel time delay [20]. Note that the results are  
 291 primarily valid in the 100 to 2475 year return periods, since this is the range chosen for the map selection optimization  
 292 problem. Recognizing that the impact varies significantly by TAZ, as indicated by Figure 3, we also examine the  
 293 accessibility loss exceedance curve for three communities: part of the San Francisco financial district, Danville, and  
 294 Pacifica (Figure 1). These correspond to TAZ IDs 2, 1161, and 224 respectively. This part of the San Francisco  
 295 financial district represents an area with relatively low expected changes in accessibility (Figure 3), whereas Danville  
 296 and Pacifica are at an elevated risk in almost all socio-economic groups (Figure 3). The general trends are corroborated  
 297 by the loss exceedance curves for these three communities (Figure 6(a) shows an example for the socio-economic  
 298 group with medium income households with fewer cars than workers). In other words, the average middle-class  
 299 person from Danville in a household with fewer cars than people who work is expected to experience travel-related  
 300 losses up to 1 *utils* per day after a rare earthquake, which he or she values at approximately \$20 per day considering  
 301 a conservative estimate of travel time and destination value. In contrast, his or her fellow Bay Area resident in San  
 302 Francisco has expected losses of only a tenth as much as experienced by a Danville resident. At return periods greater  
 303 than 100 years, we notice that Danville and Pacifica follow a similar general pattern, which differs dramatically from  
 304 that of San Francisco.

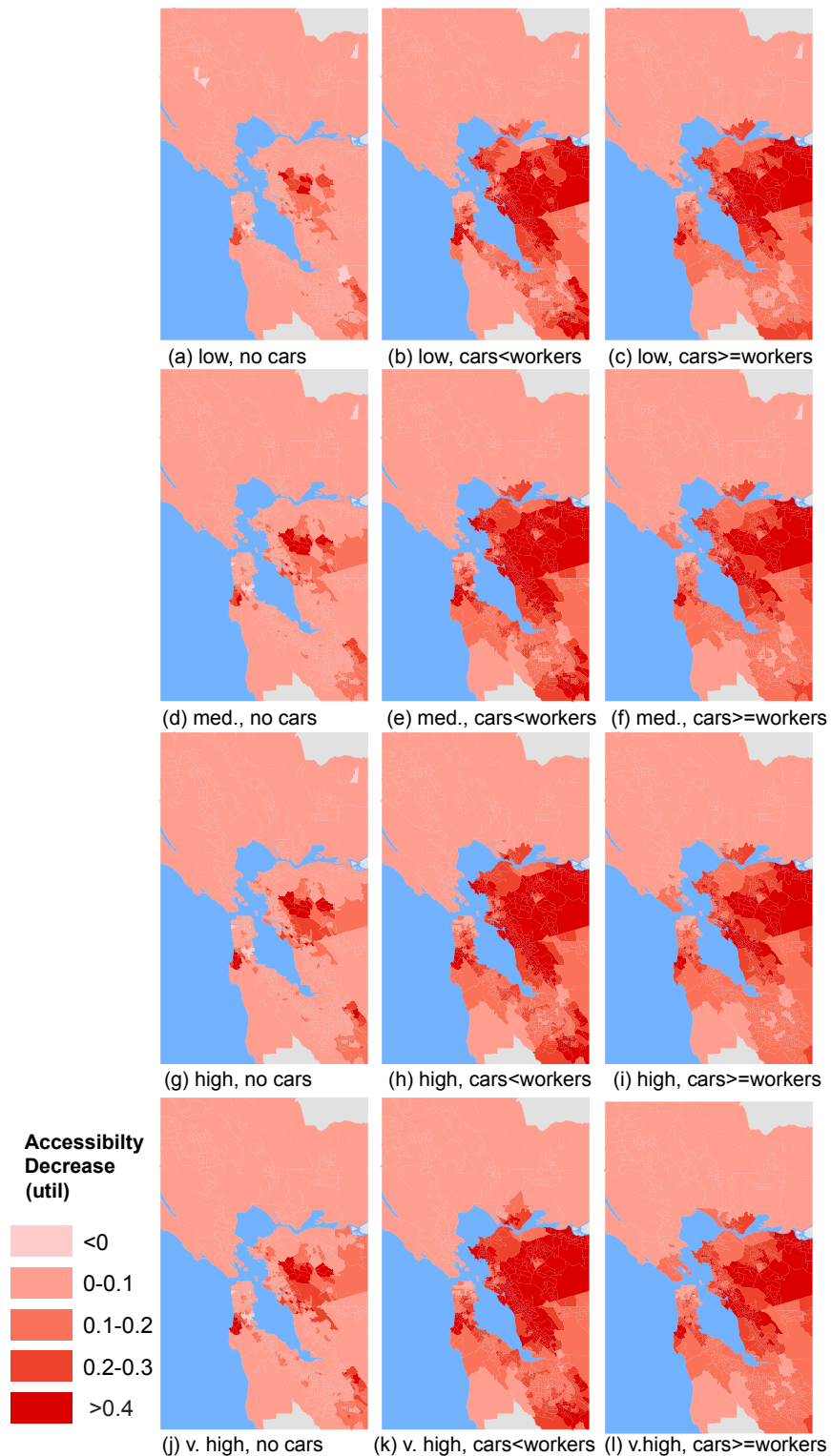


Figure 3. Expected changes in accessibility per person per day for each combination of income class and car ownership group. The darker the color, the greater the losses in accessibility.

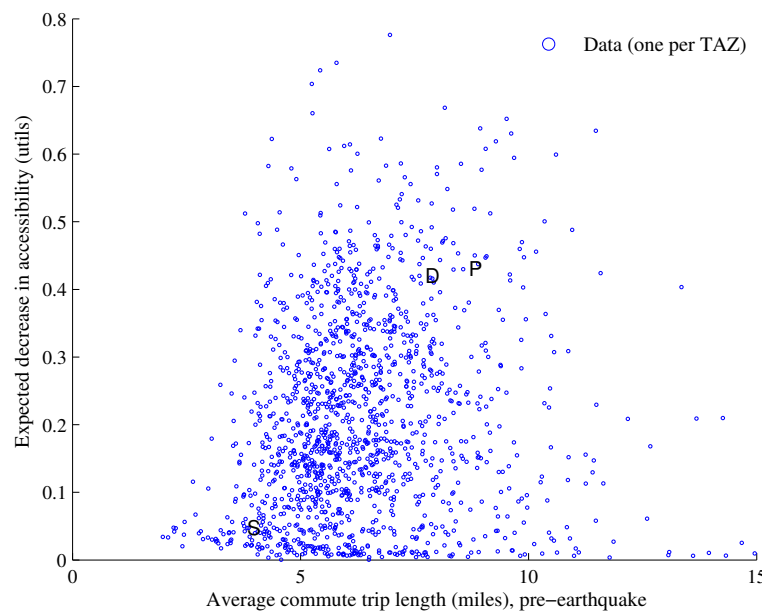


Figure 4. Trip length (pre-earthquake) versus change in total accessibility per person per day. Each dot represents one TAZ and the three case study communities, San Francisco financial district, Danville, and Pacifica are marked by **S**, **D**, and **P** respectively.

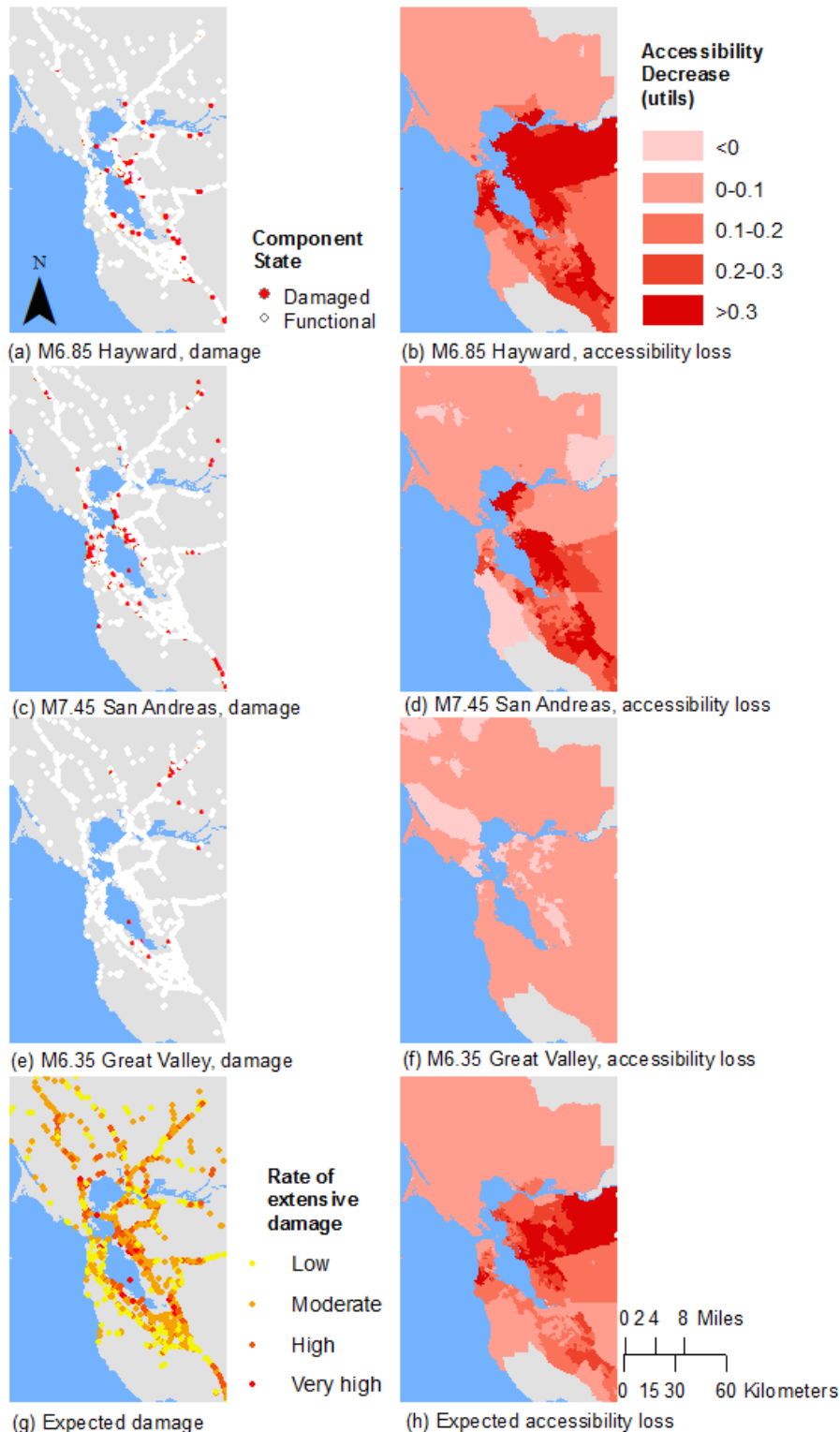


Figure 5. Bridge damage (red = damaged) and corresponding accessibility losses per person per day by TAZ for medium income households with fewer cars than workers. The bottom row has expected values calculated as a weighted average over all events.

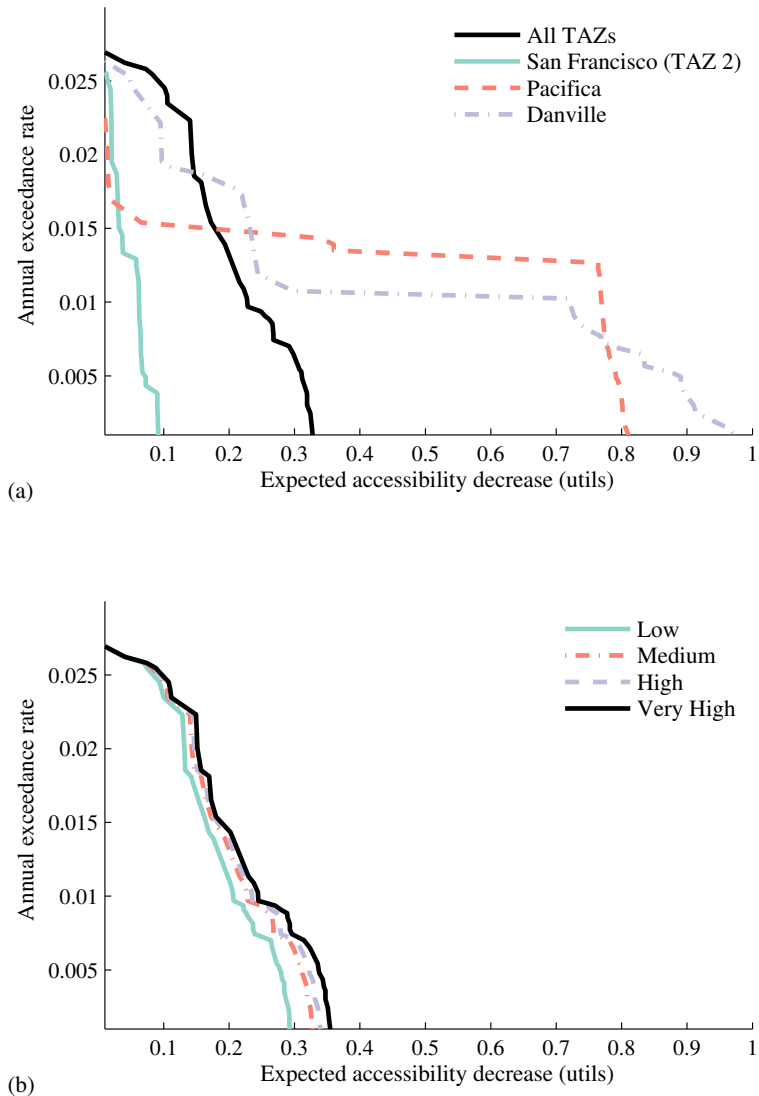


Figure 6. Accessibility annual loss exceedance curve with a comparison by (a) case study TAZs and average over all TAZs and (b) income class; all curves are in *utils* per person per day for medium income households with fewer cars than workers .

305    ***3.2. Analysis for San Francisco, CA financial district***

306    In this section, we will explore some possible explanations for why this San Francisco TAZ (Figure 1) has lower  
 307    expected accessibility losses than most other communities. First, the financial district of San Francisco differs dramatically  
 308    from many other TAZs in that the percentage of trips made by car is relatively small (38% versus an average of  
 309    85% across all TAZs). Households traveling by foot or bike will be less influenced by network damage, because the  
 310    model considers only damage to the road network and transit systems; thus, foot travel routes and travel times will not  
 311    be affected in this model. We also observe that more trips by foot and bike correspond to destinations that are closer  
 312    geographically. The impact of travel mode shift post-earthquake will be further explored in Section 3.5.

313    Second, the average time for a trip to and from work is about average for a TAZ in this region and also follows  
 314    a similar distribution to that of the other TAZs; the average trip distance for trips is only 7% lower than the average  
 315    for all trips region-wide. Since the trip time and length are relatively typical, but the accessibility is much lower than  
 316    average, the trip time and length do not explain the differences in accessibility losses.

317    In summary, the data suggests that a major cause for the low expected accessibility impact for the financial  
 318    district of San Francisco is the lower relative dependence on cars for mobility. In the next section, we will contrast  
 319    the San Francisco example with results from Pacifica, another Peninsula community that, nonetheless, is expected to  
 320    be at high risk of losses in accessibility.

321    ***3.3. Analysis for Pacifica, CA***

322    We might not suspect that Pacifica, CA would be at an extremely elevated risk of accessibility losses across most  
 323    market segments, as compared to other communities, because it is not unusually close to a major earthquake fault.  
 324    In addition, the percentage of pre-earthquake car-based trips is around average for the case study area (88% versus  
 325    an average of 85%). In contrast to most other regions, however, Pacifica is wedged between the Pacific Ocean to  
 326    the West and the coastal mountains to the East. Indeed, the main access road is California Highway 1, which has  
 327    various vulnerable bridges included in the case study dataset. There are no viable alternative routes on local roads.  
 328    Since almost all trips are by car from Pacifica and the average trip length is much longer than the region-wide average  
 329    (108% longer), the road issue is particularly serious.

330    As a comparison, consider the next main town along the Pacific coast, Half Moon Bay, about 13 miles South. Half  
 331    Moon Bay has significantly lower expected accessibility losses compared to Pacifica (0.11 *utils* per day for a person  
 332    in Half Moon Bay in middle income household with fewer cars than workers, given an event in the dataset, versus  
 333    0.43 *utils* per day for a similar person in Pacifica). While the seismic hazard is similar, the population is about one  
 334    third the size, so there is less demand for the limited road capacity [55]. Furthermore, and likely most significantly,  
 335    Half Moon Bay has a key alternative to California Highway 1, California Highway 92, which links to Silicon Valley  
 336    and the main highways of that region (US-101 and I-280). Since Pacifica, CA is unusually reliant on one road with  
 337    key vulnerabilities for access, it has an elevated risk for losses in accessibility.

338    ***3.4. Analysis for Danville, CA***

339    We will first examine the trip length characteristics for Danville, CA. The distribution of pre-earthquake commute  
 340    trips from Danville, CA is shifted towards both longer distance and longer time than the communities we have studied  
 341    so far, with a relatively higher proportion of trips taking 60–74 minutes and traveling over 40 miles than in the other  
 342    communities. The same trend holds for other trip purposes. On average, the trip lengths are longer than many other  
 343    TAZs (85% longer than the average over all trips originating from any of the TAZs). The consequence of these longer  
 344    trips is more opportunities to be impacted by a road closure, simply because more roads and bridges will be used.  
 345    Moreover, the road layout near Danville, CA mandates many highway trips, which increase the likelihood of crossing  
 346    bridges; bridges are the part of the network for which we model the vulnerability.

347    Next, we look at patterns of expected bridge damage. Bridge damage is important for many regions, including  
 348    Danville, because the percentage of car-based trips is high (85% of all trips on average, and also 85% of Danville-  
 349    origin trips). For damage map realizations for the three earthquake events we introduced—M6.85 Hayward Fault,  
 350    M7.45 San Andreas Fault, M6.35 Great Valley Fault—some bridges in the Oakland area are in the extensive or  
 351    greater damage state (Figure 5(a,c,e)). These correspond to bridge closures in the model. In addition, in the first two  
 352    cases, there are closures to the north of Danville, which represents one of the two main travel routes from Danville.  
 353    There are also scattered closed bridges to the west of Danville, likely a top travel corridor because of the workplace

354 centers in San Francisco, Oakland, and Silicon Valley (all to the west). As for transit, in the first two events, all BART  
 355 lines are closed, so there are limited alternatives to the popular road routes. The result is that the residents of Danville,  
 356 CA have reduced access to their normal destinations after all these events.

357 We can also look at bridge damage in a probabilistic event-set-based manner. The expected damage over all  
 358 events represents the annual rate of a bridge being in the extensive or complete damage state for the set of 113,940  
 359 damage maps (Figure 5(g)). This figure indicates that bridges in the Oakland-Berkeley area are particularly likely to  
 360 be damaged. We also see a few high likelihood bridges to the North of Danville. Thus, the data suggests that the  
 361 relative position of high-risk bridges to Danville contributes to this community's accessibility risk.

362 *3.5. Impact of travel mode shifts and regional variations in travel mode patterns*

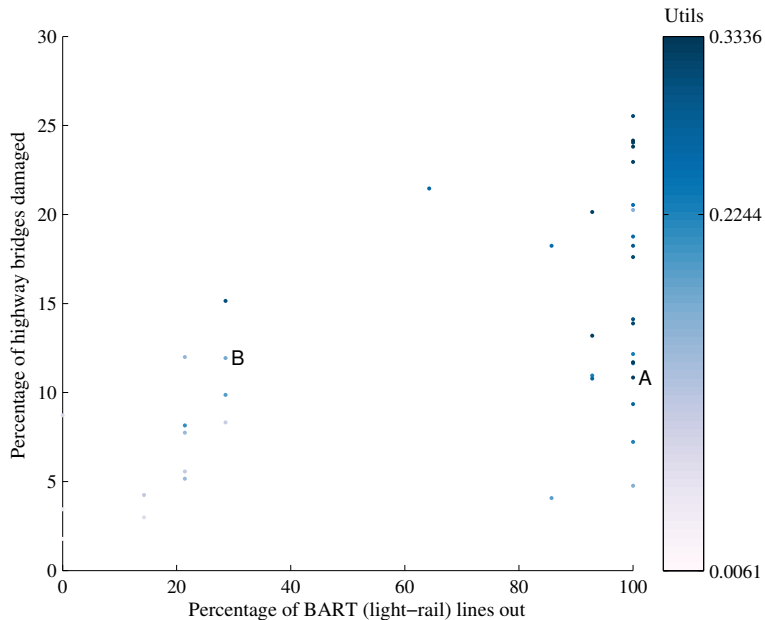


Figure 7. Percentage of BART (heavy-rail) lines not operational versus percentage of highway bridges damaged, where each data point corresponds to one earthquake damage map. The values are color-coded by the average loss in accessibility per day per person over all TAZs for households with the fewer cars than people who work. Two events discussed in this section are marked by the letters A and B.

363 First, we compare patterns of transit system damage with patterns of travel mode shifts after earthquake events.  
 364 Over all the simulated events, taking a weighted average by the annual likelihood of each event, we see a reduction in  
 365 transit ridership (25% weighted average decrease from the base case). This is not surprising. The heavy rail systems  
 366 (BART and Caltrain) are not fully operational in most of the forty simulated events (Table 2), and these have heavy  
 367 ridership. The light rail systems (VTA and Muni light rail) also suffered losses in many events (Table 2). As detailed  
 368 in [20], with regards to the other transit systems, trans-bay and cross-county bus lines were suspended in the forty  
 369 events and the baseline case; main local buses are modeled as operational, although with possible delays; and ferries  
 370 are modeled as operational. The result is an average increase in the percentage of trips by the other modes (foot, car,  
 371 and bike).

372 A notable exception is the M6.35 Great Valley, Pittsburg-Kirby Hills Fault earthquake event, as illustrated in  
 373 Figure 5(e,f). In this event, there were no line closures on the major transit systems (BART, Caltrain, Muni, and  
 374 VTA Light Rail). There were, however, some bridge closures on the highways (Figure 5(e)). The result was a slight  
 375 increase in transit ridership and also in trips by foot.

376 In general, accessibility impact grows with increasing number of damaged transit lines, particularly in combination  
 377 with high numbers of damaged bridges (Figure 7). The results do not conclusively show that transit is a key contributor  
 378 to accessibility risk, but based on individual examples, the data suggests this conclusion. For example, in the set of

Functionality	BART	Caltrain	Muni Light Rail	VTA Light Rail
Full	3	13	25	9
50-99%	10	0	15	0
1-49%	8	0	0	0
None	19	27	0	31

Table 2. Transit network functionality as a count out of the forty simulated events for BART, Caltrain, Muni Light Rail, and VTA Light Rail. Functionality is measured by the percentage of lines that are operational given a damage map (based on a ground-motion intensity map).

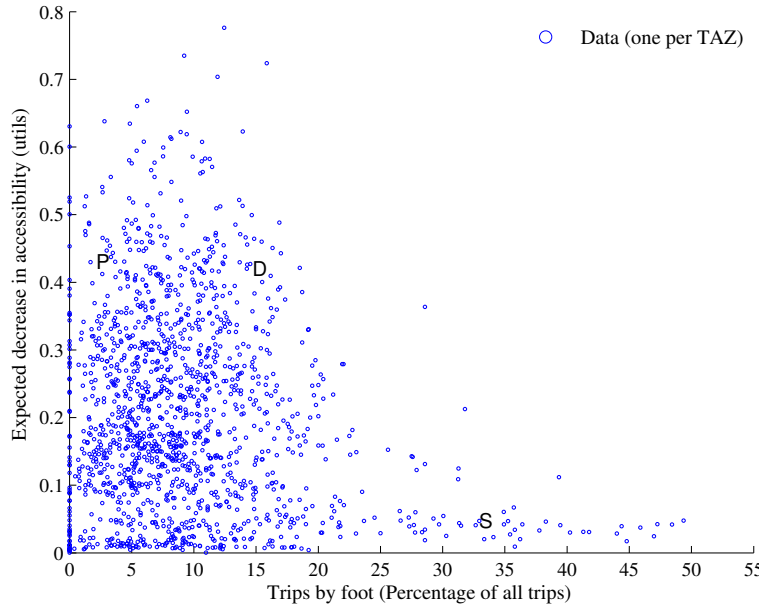


Figure 8. Percentage of total trips by foot (pre-earthquake) versus decrease in total accessibility, measured in *utils* per day (for households with the number of cars less than the number of workers). Each dot represents one TAZ and the three case study communities, San Francisco financial district, Danville, and Pacifica are marked by S, D, and P respectively.

forty events analyzed with the high-fidelity model, the M6.85 Hayward Rogers-Creek and the M7.45 Northern San Andreas Fault event both have a similar number of damaged bridges (around 11%); these are noted by points A and B respectively in Figure 7. These correspond to the bridge damage and accessibility maps in Figures 5(a,b) and 5(c,d) respectively. However, this Hayward Rogers-Creek event has significantly higher accessibility impact. Similarly, the transit impact was different. This Northern San Andreas event had only 4 of the 14 BART lines, all Caltrain, and all VTA Light Rail lines not operational, whereas this Hayward Rogers-Creek event had all 14 of the 14 BART lines, all Caltrain, all VTA Light Rail and 3 of the 8 Muni light rail lines not operational. Thus, the transit lines were impacted significantly differently. Moreover, the differences in accessibility results could not have been predicted from simpler models focusing on bridge portfolio losses, because the percent of damaged bridges was about the same, and the San Andreas event actually corresponded to a greater increase in travel time.

Second, we examine the correlation between a community's walkability, as measured by the percentage of total trips made by that travel mode, and the expected decrease in accessibility by community. We see that an increased percentage of pre-earthquake trips on foot corresponds to a lower average decrease in accessibility (Figure 8). This result corroborates the specific example of the San Francisco Financial District we saw in Section 3.2. Furthermore, on average, the number of by-foot trips slightly increases after the earthquake events where road congestion worsens. This model result is consistent with the observations after the 1995 Kobe earthquake, in which many commuters switched to walking and biking ("non-mechanized modes") in the weeks after the earthquake [7]. In conclusion, the data suggests that TAZs, i.e. communities, which have a greater walkability are also more resilient to earthquake-related accessibility risk.

398 **4. Conclusions**

399 Here we have shown how mode-destination accessibility links post-earthquake infrastructure damage to the impact  
 400 on human welfare and enables identifying at-risk geographic and demographic groups in a region. Adopting this  
 401 state-of-the-art performance metric from the urban planning community, we have illustrated its use for seismic risk  
 402 assessment and mitigation through a case study of the San Francisco Bay Area. For the case study, we consider a  
 403 set of 40 hazard-consistent earthquake scenarios, ground-motion intensity maps, and damage maps. For each damage  
 404 map, we processed the data for analysis in a high-fidelity, activity-based travel model that includes the road network,  
 405 transit networks, walking and biking options, variable travel demand, and mode choice. We used this data and model  
 406 to compute the mode-destination accessibility, a performance measure for each community and each socio-economic  
 407 group (defined by income class and car ownership).

408 We saw stark differences in accessibility from location to location. Specifically, we found that areas in the suburbs,  
 409 such as the far East Bay, South San Jose and select communities just south of San Francisco, were particularly at risk.  
 410 We found that these geographic trends persisted across income classes and car ownership groups. Nonetheless, on  
 411 average, higher income households with more cars than workers had the highest risk across the studied socio-economic  
 412 groups. One key reason is the geographic clustering of these households in higher-risk areas. Another factor is that  
 413 these households tend to take longer daily trips, thus crossing more roads and bridges and possibly increasing the  
 414 likelihood of disruption.

415 This study also demonstrated that travel modes shift after an earthquake, and communities who can more easily  
 416 make these adjustments are generally predicted to experience lower post-earthquake losses in accessibility. The results  
 417 suggest that the walkability of a community, as measured by the percentage of pre-earthquake trips by foot, is closely  
 418 linked to reduced accessibility risk. We also found that one adaptation measure after major earthquakes is an increased  
 419 likelihood to walk or bike. We also found that in almost all of the simulated earthquake events, the transit system,  
 420 particularly the heavy rail (BART and Caltrain) lines, is predicted by this model to be severely impacted. The result  
 421 is a reduced mode share for transit and increased trips by the other modes (car, walk, bike). Thus, this study suggests  
 422 that not including transit can lead to an unconservative estimate of seismic risk of transportation systems. The model  
 423 shows, however, that when transit is not damaged—which is very rare for this case study—ridership increases.

424 In conclusion, mode-destination accessibility offers important applications for further investigation into the impact  
 425 to human welfare of engineering losses and mitigation efforts. This work lays the foundation for future work in risk  
 426 mitigation and policy to reduce the vulnerability of at-risk communities. It also suggests that initiatives making  
 427 communities more conducive for cycling and walking to work can increase resiliency.

428 **References**

- 429 [1] L. Dueñas-Osorio, J. I. Craig, B. J. Goodno, Seismic response of critical interdependent networks, *Earthquake Engineering & Structural*  
   *Dynamics* 36 (2) (2007) 285306. doi:10.1002/eqe.626.
- 430 [2] S. E. Chang, M. Shinozuka, J. E. Moore, Probabilistic earthquake scenarios: Extending risk analysis methodologies to spatially distributed  
   systems, *Earthquake Spectra* 16 (3) (2000) 557–572. doi:10.1193/1.1586127.
- 431 [3] R. C. Bolin, L. Stanford, *The Northridge earthquake: vulnerability and disaster*, Routledge, London; New York, 1998.
- 432 [4] The World Bank and the United Nations, *Natural hazards, unnatural disasters: the economics of effective prevention*, Tech. rep., The World  
   Bank, Washington D.C. (2010).
- 433 [5] California. Dept. of Transportation. Post Earthquake Investigation Team, *Northridge earthquake, 17 January 1994: PEQIT report*, California  
   Department of Transportation, Division of Structures, Sacramento, 1994.
- 434 [6] K. J. Tierney, Business Impacts of the Northridge Earthquake, *Journal of Contingencies and Crisis Management* 5 (2) (1997) 87–97.  
   doi:10.1111/j.1468-5973.00040.
- 435 [7] P. Gordon, H. W. Richardson, B. Davis, Transport-related impacts of the Northridge earthquake, National Emergency Training Center, 1998.
- 436 [8] A. Kiremidjian, J. Moore, Y. Y. Fan, O. Yazlali, N. Basöz, M. Williams, Seismic risk assessment of transportation network systems, *Journal*  
   *of Earthquake Engineering* 11 (3) (2007) 371–382. doi:10.1080/13632460701285277.
- 437 [9] N. Jayaram, J. W. Baker, Efficient sampling and data reduction techniques for probabilistic seismic lifeline risk assessment, *Earthquake*  
   *Engineering & Structural Dynamics* 39 (10) (2010) 1109–1131. doi:10.1002/eqe.988.
- 438 [10] C. S. Oliveira, M. A. Ferreira, F. M. d. S., The concept of a disruption index: application to the overall impact of the July 9, 1998 Faial  
   *earthquake* (Azores islands), *Bulletin of Earthquake Engineering* 10 (1) (2012) 7–25. doi:10.1007/s10518-011-9333-8.
- 439 [11] P. Bocchini, D. M. Frangopol, Restoration of bridge networks after an earthquake: Multicriteria intervention optimization, *Earthquake Spectra*  
   28 (2) (2012) 426–455. doi:10.1193/1.4000019.
- 440 [12] F. Cavalieri, P. Franchin, P. Gehl, B. Khazai, Quantitative assessment of social losses based on physical damage and interaction with infrastruc-  
   tural systems, *Earthquake Engineering & Structural Dynamics* 41 (11) (2012) 1569–1589. doi:10.1002/eqe.2220.
- 441 [13] F. S. Chapin, *Urban land use planning*, University of Illinois Press, 1970.

- [14] D. A. Niemeier, Accessibility: an evaluation using consumer welfare, *Transportation* 24 (4) (1997) 377396.
- [15] K. T. Geurs, B. van Wee, Accessibility evaluation of land-use and transport strategies: review and research directions, *Journal of Transport Geography* 12 (2) (2004) 127–140. doi:10.1016/j.jtrangeo.2003.10.005.
- [16] S. L. Handy, D. A. Niemeier, Measuring accessibility: an exploration of issues and alternatives, *Environment and Planning A* 29 (7) (1997) 11751194.
- [17] I. Hernandez-Fajardo, L. Dueñas-Osorio, Probabilistic study of cascading failures in complex interdependent lifeline systems, *Reliability Engineering & System Safety* 111 (2013) 260–272. doi:10.1016/j.ress.2012.10.012.
- [18] M. Miller, J. Baker, Ground-motion intensity and damage map selection for probabilistic infrastructure network risk assessment using optimization, in review (2014).
- [19] R. Cervero, K.-L. Wu, Polycentrism, commuting, and residential location in the San Francisco Bay area, *Environment and Planning A* 29 (5) (1997) 865–886.
- [20] M. Miller, Seismic risk assessment of complex transportation networks, PhD thesis, Stanford University (2014).
- [21] D. M. Boore, G. M. Atkinson, Ground-motion prediction equations for the average horizontal component of PGA, PGV, and 5%-damped PSA at spectral periods between 0.01 s and 10.0 s, *Earthquake Spectra* 24 (1) (2008) 99–138.
- [22] N. Abrahamson, W. Silva, Summary of the Abrahamson & Silva NGA Ground-Motion Relations, *Earthquake Spectra* 24 (1) (2008) 67–97. doi:10.1193/1.2924360.
- [23] B. Chiou, R. R. Youngs, An NGA model for the average horizontal component of peak ground motion and response spectra, *Earthquake Spectra* 24 (1) (2008) 173–215. doi:10.1193/1.2894832.
- [24] K. W. Campbell, Y. Bozorgnia, NGA ground motion model for the geometric mean horizontal component of PGA, PGV, PGD and 5% damped linear elastic response spectra for periods ranging from 0.01 to 10s, *Earthquake Spectra* 24 (1) (2008) 139–171. doi:10.1193/1.2857546.
- [25] J. W. Baker, C. A. Cornell, Which spectral acceleration are you using?, *Earthquake Spectra* 22 (2) (2006) 293–312. doi:10.1193/1.2191540.
- [26] R. Foulser-Piggott, P. J. Stafford, A predictive model for Arias intensity at multiple sites and consideration of spatial correlations, *Earthquake Engineering & Structural Dynamics* 41 (3) (2012) 431451. doi:10.1002/eqe.1137.
- [27] Y. Han, R. A. Davidson, Probabilistic seismic hazard analysis for spatially distributed infrastructure, *Earthquake Engineering & Structural Dynamics* 41 (15) (2012) 2141–2158. doi:10.1002/eqe.2179.
- [28] N. Jayaram, J. W. Baker, Correlation model for spatially distributed ground-motion intensities, *Earthquake Engineering & Structural Dynamics* 38 (15) (2009) 1687–1708. doi:10.1002/eqe.922.
- [29] E. H. Field, T. H. Jordan, C. A. Cornell, OpenSHA: a developing community-modeling environment for seismic hazard analysis, *Seismological Research Letters* 74 (4) (2003) 406–419. doi:10.1785/gssrl.74.4.406.
- [30] M. Shinozuka, Y. Murachi, X. Dong, Y. Zhou, M. J. Orlitzkowsky, Effect of seismic retrofit of bridges on transportation networks, *Earthquake Engineering and Engineering Vibration* 2 (2) (2003) 169–179. doi:10.1007/s11803-003-0001-0.
- [31] E. H. Field, T. E. Dawson, K. R. Felzer, A. D. Frankel, V. Gupta, T. H. Jordan, T. Parsons, M. D. Petersen, R. S. Stein, R. J. Weldon, C. J. Wills, Uniform California Earthquake Rupture Forecast, Version 2 (UCERF 2), *Bulletin of the Seismological Society of America* 99 (4) (2009) 2053–2107. doi:10.1785/0120080049.
- [32] D. J. Wald, T. I. Allen, Topographic slope as a proxy for seismic site conditions and amplification, *Bulletin of the Seismological Society of America* 97 (5) (2007) 1379–1395. doi:10.1785/0120060267.
- [33] N. Basöz, J. Mander, Enhancement of the highway transportation lifeline module in HAZUS, Tech. rep., Final Pre-Publication Draft (#7) prepared for the National Institute of Building Sciences (NIBS) (1999).
- [34] K. N. Ramanathan, Next generation seismic fragility curves for California bridges incorporating the evolution in seismic design philosophy, PhD thesis, Georgia Institute of Technology (2012).
- [35] R. Lee, A. S. Kiremidjian, Uncertainty and correlation for loss assessment of spatially distributed systems, *Earthquake Spectra* 23 (4) (2007) 753–770. doi:10.1193/1.2791001.
- [36] S. Werner, C. Taylor, S. Cho, J. Lavoie, REDARS 2 methodology and software for seismic risk analysis of highway systems (technical manual), Tech. rep., Seismic Systems & Engineering Analysis for MCEER, Oakland, CA (2006).
- [37] Caltrans, Caltrans Seismic Design Criteria Version 1.7, Tech. Rep. SDC 1.7, California Department of Transportation, Sacramento, CA (2013).
- [38] Bechtel/HNTB Team, Design Criteria Volume I, Version 1.2, Tech. rep., San Francisco Bay Area Rapid Transit District, San Francisco Bay Area Rapid Transit District Earthquake Safety Program (2008).
- [39] N. Kurtz, J. Song, P. Gardoni, Time-varying seismic reliability analysis of representative US west coast bridge transportation networks, in: G. Deodatis, B. R. Ellingwood, D. M. Frangopol (Eds.), *Safety, Reliability, Risk and Life-Cycle Performance of Structures and Infrastructures*, CRC Press, 2014, pp. 655–662.
- [40] J. Ghosh, K. Rokneddin, J. E. Padgett, L. Dueas-Osorio, Seismic reliability assessment of aging highway bridge networks with field instrumentation data and correlated failures. I: Methodology, *Earthquake Spectra* 30 (2) (2013) 795–817. doi:10.1193/040512EQS155M.
- [41] S. Pugh, Construction statistics, Tech. rep., California Department of Transportation Division of Engineering Services (2012).
- [42] K. Kockelman, Travel Behavior as Function of Accessibility, Land Use Mixing, and Land Use Balance: Evidence from San Francisco Bay Area, *Transportation Research Record: Journal of the Transportation Research Board* 1607 (-1) (1997) 116–125. doi:10.3141/1607-16.
- [43] P. Waddell, F. Nourzad, Incorporating nonmotorized mode and neighborhood accessibility in an integrated land use and transportation model system, *Transportation Research Record: Journal of the Transportation Research Board* 1805 (-1) (2002) 119–127. doi:10.3141/1805-14.
- [44] C. F. Manski, *Structural analysis of discrete data with econometric applications*, MIT Press, 1981.
- [45] K. A. Small, H. S. Rosen, Applied welfare economics with discrete choice models, *Econometrica* 49 (1) (1981) 105–130. doi:10.2307/1911129.
- [46] D. Ory, Personal communication (2013).
- [47] United States Department of Transportation, Revised departmental guidance: valuation of travel time in economic analysis, US Department of Transportation, Washington, DC.
- [48] G. Erhardt, P. Brinckerhoff, D. Ory, A. Sarvepalli, J. Freedman, J. Hood, B. Stabler, MTC's Travel Model One: applications of an activity-

- 517 based model in its first year, in: Innovations in Travel Modeling 2012, Tampa, Florida, 2012, p. 9.
- 518 [49] P. Waddell, UrbanSim: modeling urban development for land use, transportation, and environmental planning, Journal of the American  
519 Planning Association 68 (3) (2002) 297–314. doi:10.1080/01944360208976274.
- 520 [50] W. Davidson, P. Vovsha, J. Freedman, R. Donnelly, CT-RAMP family of activity-based models, in: Proceedings of the 33rd Australasian  
521 Transport Research Forum (ATRF), Canberra, Australia, 2010, p. 15.
- 522 [51] H. Wakabayashi, H. Kameda, Network performance of highway systems under earthquake effects: a case study of the 1989 Loma Prieta  
523 earthquake, in: Proceedings US-Japan Workshop on Earthquake Disaster Prevention for Lifeline Systems, 1992, pp. 215–232.
- 524 [52] A. A. Hagberg, D. A. Schult, P. J. Swart, Exploring network structure, dynamics, and function using NetworkX, in: Proceedings of the 7th  
525 Python in Science Conference (SciPy2008), Pasadena, CA USA, 2008, p. 1115.
- 526 [53] H.-W. Lim, J. Song, N. Kurtz, Seismic reliability assessment of lifeline networks using clustering-based multi-scale approach, in review  
527 (2014).
- 528 [54] P. Wang, T. Hunter, A. M. Bayen, K. Schechtner, M. C. Gónzalez, Understanding road usage patterns in urban areas, Scientific Reports 2.  
529 doi:10.1038/srep01001.
- 530 [55] U.S. Bureau of the Census, United States Census 2010, Tech. rep., U.S. Census Bureau, Washington D.C. (2010).